Communication

Low-Frequency Content of THz Emission from Two-Color Femtosecond Filament

Daniil E. Shipilo [1,*] **, Nikolay A. Panov** [1,2] **, Irina A. Nikolaeva** [1,2] **, Alexander A. Ushakov** [3] **,**
Pavel A. Chizhov [3,4] **, Kseniia A. Mamaeva** [3] **, Vladimir V. Bukin** [3] **, Sergey V. Garnov** [3] **and Olga G. Kosareva** [1,2]

[1] P.N. Lebedev Physical Institute of the Russian Academy of Sciences, 119991 Moscow, Russia; napanov@ilc.edu.ru (N.A.P.); nikolaevaia@lebedev.ru (I.A.N.); kosareva@physics.msu.ru (O.G.K.)
[2] Faculty of Physics, Lomonosov Moscow State University, 119991 Moscow, Russia
[3] Prokhorov General Physics Institute of the Russian Academy of Sciences, 119991 Moscow, Russia; ushakov.aleksandr@physics.msu.ru (A.A.U.); pvch@kapella.gpi.ru (P.A.C.); mamaeva@physics.msu.ru (K.A.M.); vbkn@kapella.gpi.ru (V.V.B.); garnov@kapella.gpi.ru (S.V.G.)
[4] Russian Institute for Scientific and Technical Information, 125315 Moscow, Russia
[*] Correspondence: schipilo.daniil@physics.msu.ru

Abstract: We experimentally investigate the low-frequency (below 1 THz) spectral content of broadband terahertz (THz) emission from two-color femtosecond filament formed by the 2.7-mJ, 40-fs, 800 + 400-nm pulse focused into air. For incoherent detection, we screened the Golay cell by the bandpass filters and measured the THz angular distributions at the selected frequencies $\nu = 0.5, 1, 2$ and 3 THz. The measured distributions of THz fluence were integrated over the forward hemisphere taking into account the transmittance of the filters, thus providing the estimation of spectral power at the frequencies studied. The spectral power decreases monotonically with the frequency increasing from 0.5 to 3 THz, thus showing that the maximum of THz spectrum is attained at $\nu \leq 0.5$ THz. The THz waveform measured by electro-optical sampling (EOS) based on ZnTe crystal and transformed into the spectral domain shows that there exists the local maximum of the THz spectral power at $\nu \approx 1$ THz. This disagrees with monotonic decrease of THz spectral power obtained from the filter-based measurements. We have introduced the correction to the spectral power reconstructed from EOS measurements. This correction takes into account different focal spot size for different THz frequencies contained in the broadband electromagnetic pulse. The corrected EOS spectral power is in semi-quantitative agreement with the one measured by a set of filters.

Keywords: two-color femtosecond filament; terahertz radiation; low-frequency terahertz content

1. Introduction

Two-color femtosecond filament [1] with the intensity of ∼100 TW/cm² [2–4], the beam diameter of 50–100 μm [5–7], and the plasma density of 10^{15}–10^{19} cm^{-3} [8,9] is a terahertz (THz) source with the most broadband spectrum up to 50–100 THz [10–12], depending on the pump pulse duration [13]. The high-frequency THz emission from two-color filament has been studied in details both experimentally and theoretically [13–17]. So, the angular distribution in the range of frequencies $\nu \gtrsim 5$ THz is conical [16,18–21], but the shape of directional diagrams at lower frequencies is still debated [22]. Indeed, the experiments [21–23] show the unimodal on-axis angular distribution of THz emission from two-color filament for $\nu \lesssim 3$ THz. However, in other experiments [24–26], the conical divergence of THz radiation was observed.

The spectral distribution of the low-frequency THz emission from a two-color filament is still unknown. Even the position of the low-frequency maximum ν_{max} in the THz spectra measured in the close conditions (pulse energy and duration, geometry of the experiment etc.) can vary by an order of magnitude from one experiment to another. We collected the corresponding data in Table 1, which shows that as the pump pulse duration varies in the range of 30–50 fs, the position of the spectral maximum travels in a wide frequency

range from 0.4 THz [27] to 13 THz [28]. Self-consistent numerical simulations based on Unidirectional pulse propagation Equation (UPPE [29]) predict the maximum of THz spectrum at the frequency of about a few hundreds of gigahertz [16,17].

Table 1. The frequency of maximum ν_{max} in the THz spectra measured in different experiments in the conditions close to the ones of our experiment.

Pulse Duration, fs	Pulse Energy, mJ	Focusing Conditions	Detection Method	ν_{max}, THz	Ref.
32	~1	$f = 15$ cm	EOS	2.9	[13]
32	0.7	$f = 15$ cm	ABCD	4.4	[30]
32	0.7	—	ABCD	~5	[31]
35	2	$f = 25$ cm	EOS	0.4	[27]
35	~3	$f/15$	Interferometer	13	[28]
40	0.7–2	$f = 15$–25 cm	EOS	~1	[32]
40	~1	$f = 15$ cm	EOS	2.3	[13]
40	2.3	$f = 20$ cm	EOS (ZnTe) EOS (GaP) ABCD Interferometer	1.7 2.2 3.4 7	[33]
40	1–6	$f/10$	Interferometer	5–10	[34]
50	0.5	$f = 30$ cm	EOS	0.4	[35]
50	1.15	$f/80$	EOS	~0.5	[36]
50	2.5	$f/40$–$f/4$	EOS	0.5–0.7	[37]
50	1.7	$f = 20$ cm	EOS	~1	[38]
50	~1	—	ABCD EOS	0.55 1.7	[31]

　　This large spreading of experimentally obtained frequencies ν_{max} can be attributed to the extreme broadness of the spectrum of THz emission from two-color filament. Different components of the THz spectrum have different divergence diagrams. As the result, the THz focal spot size varies significantly across the spectrum. This focal spot size variation affects the collection of THz radiation by coherent detection schemes, in particular, electro-optical sampling EOS [39] and air-biased coherent detection ABCD [40]. Both methods require overlap between the probe optical pulse and the focused THz pulse. The THz spot transverse size is of order of THz wavelength or larger, and, therefore, exceeds the typical ~1 mm (or even less in case of ABCD detection) diameter of the probe beam [41,42]. For example, at the low THz frequency $\nu \lesssim 0.5$ THz with the corresponding wavelength larger than ~600 μm, the THz beam size in the focus is equal or larger than 1 mm. As a result, a significant fraction of the THz beam does not overlap with the probe, and the coherent time domain sampling (TDS) underestimates the low-frequency THz content [43].

　　It should be noted that this underestimation does not prevent the time-domain sampling from being an excellent tool in THz spectroscopy [44]. Indeed, through the comparison of the spectrum of THz radiation transmitted through the substance and the one of the reference THz signal, TDS provides the information about both real and imaginary parts of the dielectric susceptibility [39]. The low in the amplitude half-cycle electric field in a standard EOS crystal ZnTe (89 kV/cm for a 1 mm thickness [45]) makes the registration of a weak THz signal possible. Using EOS, Zhong et al. recorded the THz spectra of explosives from the distance of 30 m in the atmosphere [46]. The EOS scheme can be adapted for 2*D* frequency-resolved imaging of organic substances [47]. The ABCD technique was applied

to broadband THz spectroscopy [48,49]. The dispersion of TDS sensitivity becomes a problem only if one decides to characterize the THz source rather than the sample.

The incoherent methods of THz spectra registration based on the Michelson interferometer coupled to a THz powermeter (a bolometer or a Golay cell) are aimed at the high-frequency THz content [33]. The THz spectra measured by these devices have the maximum at high THz frequencies $\nu_{max} \geq 5$ THz, see Table 1. The strongly divergent low-frequency THz radiation diffracts out of the aperture of the interferometer mirrors and does not enter the powermeter. Therefore, the low-frequency THz content is underestimated in such interferometric measurements as well.

The purpose of this work is to study experimentally the low-frequency ($\nu \lesssim 1$ THz) spectral content of the broadband THz emission from two-color femtosecond filament, formed in air by 2.7-mJ, 40-fs, $800 + 400$-nm pulse in the vicinity of 20-cm geometrical focus. To reconstruct the spectral components of THz emission from two-color filament, we measured the angular distributions of the THz radiation by rotation of the Golay cell, the entrance window of which was screened by the bandpass filters centered at 0.5, 1, 2 and 3 THz (see Figure 1a). The spectrum reconstructed from THz angular distributions was compared with the one measured by electro-optical sampling for the same two-color filament (see Figure 1b). The comparison shows relatively low power at the frequency below 1 THz in the case of EOS measurement. We found that the qualitative agreement between the two spectra is achieved if the spectrum obtained from EOS is corrected based on the convolution between the optical probe and THz pump pulse in ZnTe crystal.
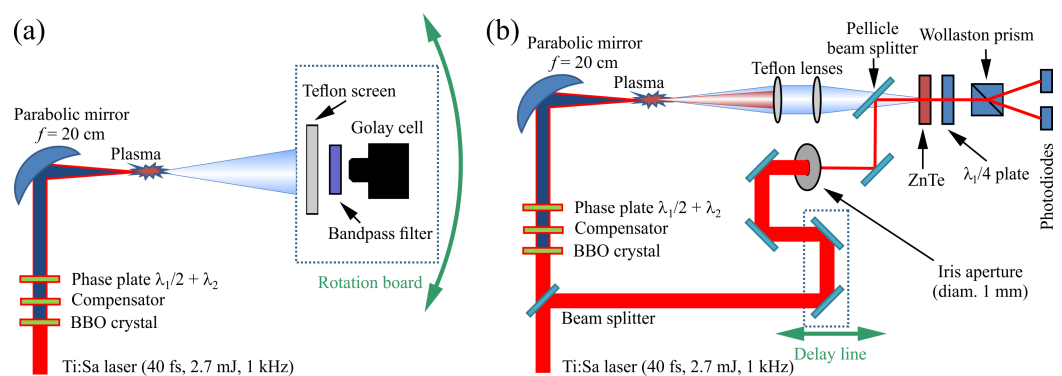

Figure 1. Experimental schemes. (**a**) Angular distribution measurements. Golay cell with a bandpass filter and teflon screen is mounted on the board rotating around the geometrical focus along the green arc with arrows on both sides. (**b**) Time-domain measurements. A focused THz beam is combined on the ZnTe crystal with a probe pulse, the time delay of which is varied by moving the delay line along the green line with arrows on both sides.

2. Materials and Methods

In the experiment we used the laser pulses delivered by Ti:Sapphire laser system Spectra Physics Spitfire Pro XP centred at the wavelength $\lambda_1 = 800$ nm with the energy up to 2.7 mJ, FWHM duration of 40 fs and beam diameter of 12 mm (at e^{-2} level) at 1 kHz repetition rate. To form the two-color filament we inserted a BBO crystal (I-type, 100-μm thickness, 10% efficiency) into the pump beam thus providing generation of the second harmonic radiation centered at $\lambda_2 = 400$ nm (Figure 1). The BBO crystal was adjusted to maximize the second harmonic yield. Behind the BBO crystal, polarization of the 400-nm radiation was oriented perpendicularly to the one of the 800-nm pump. Similarly to our work [23], a compensator plate decreased the group delay between the fundamental (λ_1) and the second (λ_2) harmonic pulses. A dual wavelength phase plate ("$\lambda_1/2 + \lambda_2$" in Figure 1) served to align the polarization vectors of the harmonic pulses in order to maximize the THz yield. Thereby, both harmonics had the same vertical linear polarization direction and zero group delay between themselves in the filament. After the dual wavelength phase plate the two-color beam was focused into the atmospheric

air by the off-axis parabolic mirror with the focal length $f = 20$ cm. In the vicinity of the geometrical focus, the ∼10-mm two-color filament was formed. It was the source of THz radiation, which spectral content was studied in our experiment.

We measured the spectral content of THz emission from two-color laser-induced plasma using two different techniques. In the first case (Figure 1a), we screened the Golay cell by the teflon plate (to block laser radiation) and the bandpass filters (Tydex [50]) centered at the frequencies $\nu = 0.5, 1, 2$ and 3 THz. The transmittance spectra provided by the manufacturer for our filters are shown in Figure 2 by the colored areas. We rotated the Golay cell placed at a distance of 20 cm from the geometrical focus around the vertical axis by the angle θ relative to the laser beam axis with the step $\Delta\theta = 2.5°$ (Figure 1a). With this setup we recorded the angular distributions of THz fluence $F(\theta)$ at different frequencies ν. In these measurements the Pockels cell located in the regenerative amplifier provided the modulation of generated THz emission with a frequency of 20 Hz. The resulting THz signal was registered by means of synchronous detection technique using lock-in amplifier. The measured dependencies $F(\theta)$ were processed according to Ref. [51] to obtain the power S of the spectral components at the set of frequencies studied.
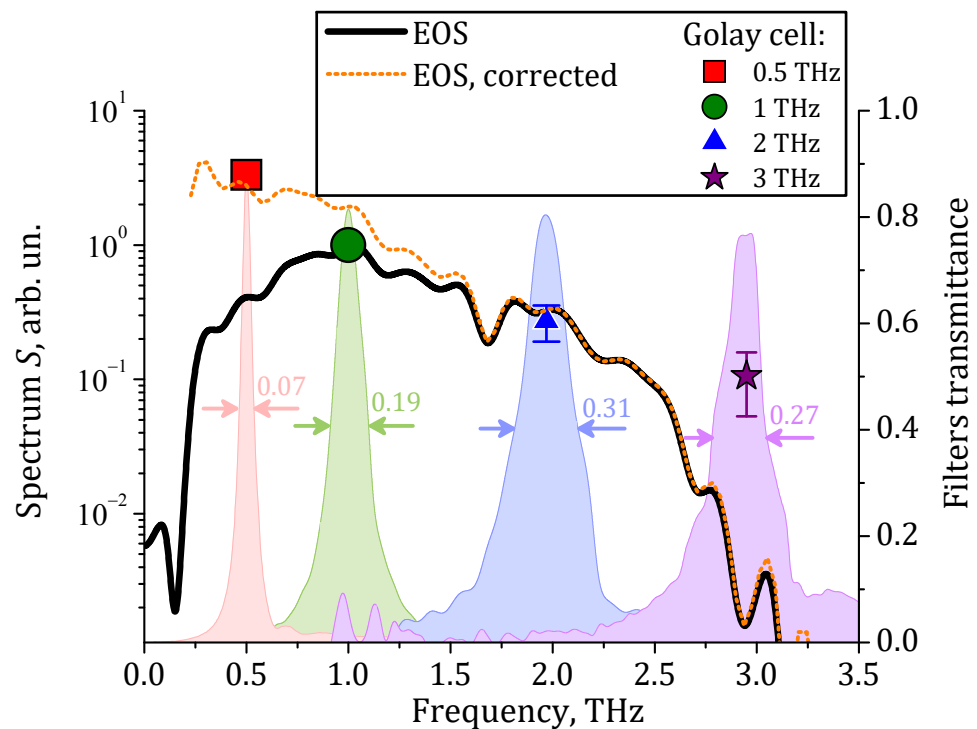

Figure 2. Spectrum of THz radiation obtained after integration of measured by the Golay cell with bandpass filters angular distributions of THz spectral intensity $I(\theta)$ (symbols, left axis) and spectrum measured by EOS (black curve, left axis). The orange dotted curve (left axis) is the spectrum calculated from the one measured by EOS (the black solid curve) using the EOS sensitivity from Appendix A, Equation (A11). The colored areas (right axis) show THz bandpass filters transmittance spectra. Arrows with numbers indicate their full width at half maximum $\Delta\nu$ in *terahertz*.

In the second case (Figure 1b), we measured THz waveforms using a standard time-domain system based on the electro-optics sampling technique (EOS [39]). The system consisted of the ZnTe crystal ($10 \times 10 \times 0.5$ mm^3, ⟨110⟩ cut), the quarterwave plate ("$\lambda_1/4$" in Figure 1b), the Wollaston prism, and two photodiodes. This setup registered the radiation in the spectral range from ∼0.2 to ∼3 THz. Two 50-mm in diameter teflon lenses with the foci of 6 and 10 cm collimated the THz radiation and focused it onto the ZnTe crystal, respectively (Figure 1b). Optical probe pulse passed through a variable delay line and then was combined with the THz pulse on a lavsan pellicle. So as to decrease a fluctuation

of registered signal, we apertured the collimated probe beam down to 1 mm in diameter. By the variation of the delay between the probe and THz pulses, we measured the THz waveforms. The THz spectrum was reconstructed from the measured waveform using the Fourier transform.

3. Results and Discussion

Figure 3a shows the dependence of the THz fluence F on the polar angle θ measured by the Golay cell at the frequency $\nu = 0.5$ THz (red squares), 1 THz (green circles), 2 THz (blue triangles) and 3 THz (violet stars). Angular distributions $F(\theta)$ get narrower with the frequency increase in reasonable agreement with the well-known law [52] for the divergence angle

$$\delta \propto \sqrt{\nu^{-1}} \qquad (1)$$

of electromagnetic waves emitted from an extended source, see Figure 4. Equation (1) is usually used in the studies of THz emission from a single-color filament [53–55], however, is valid in the case of two-color filament [18], and even for wire lasers [56].
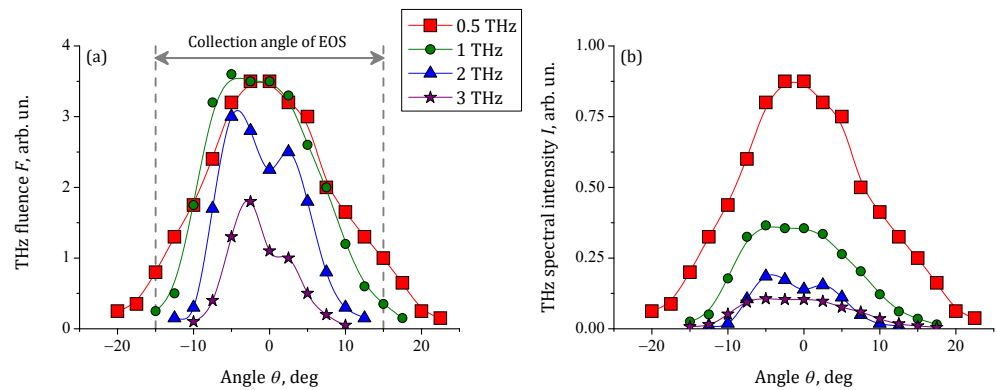

Figure 3. Angular distributions of (**a**) THz fluence $F(\theta)$ measured by the Golay cell with bandpass filters at the frequencies $\nu = 0.5$ THz (red squares), 1 THz (green circles), 2 THz (blue triangles), 3 THz (violet stars) and (**b**) THz spectral intensity $I(\theta)$ obtained from (**a**) by the correction to the maximal transmittance of the filters T and their bandwidth $\Delta\nu$, see Equation (2).
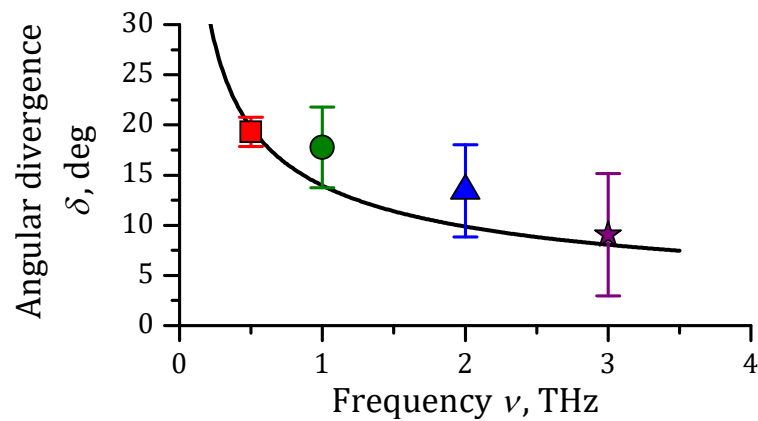

Figure 4. Dependence of the angular divergence δ of THz radiation on frequency ν estimated from angular distributions of THz fluence $F(\theta)$ (symbols). Black solid curve shows the fit of the angular divergence by Equation (1). Symbols correspond to the ones in Figure 3.

Bandpass filters centered at different frequencies ν have different transmittance spectra, see colored areas in Figure 2. So, to compare the amplitudes of THz signal measured with

different filters, we recalculated the measured THz fluence F (see Figure 3a) into the THz spectral intensity I (see Figure 3b) according to the equation:

$$I(\nu,\theta) = \frac{F(\nu,\theta)}{T(\nu)\Delta\nu(\nu)}. \tag{2}$$

Equation (2) takes into account the transmittance of the filters T, their bandwidth $\Delta\nu$ (see colored areas in Figure 2) and the constant spectral sensitivity of the Golay cell within the range of frequency studied, that is from 0.5 to 3 THz. The maximal transmittance T slightly changes with the central frequency of the bandpass filter ν. At the same time, the filter bandwidth $\Delta\nu$ increases fourfold with the central frequency ν increase from 0.5 to 3 THz (cf. red and violet colored areas in Figure 2). This results in monotonic decrease in the angularly-resolved THz spectral intensity I with the frequency increase (Figure 3b). In contrast, the measured THz fluence profiles F have almost the same amplitude for all the frequencies studied (Figure 3a).

According to 2D measurements of the THz transverse spatial distribution [18,19,57], the latter is axially symmetrical in the case of geometrical focusing into air of the moderate-power pulse [58]. Assuming axial symmetry of THz beam in our experiments, we integrate the directional diagrams $I(\nu,\theta)$ over the whole forward hemisphere to obtain the spectral power of THz radiation $S(\nu)$:

$$S(\nu) = \Delta\theta \sum_p I(\nu,p\Delta\theta)|\sin(p\Delta\theta)|, \tag{3}$$

where $\Delta\theta = 2.5°$ and the integer index p runs over the angular positions of the Golay cell. The spectral powers $S(\nu)$ calculated from Equation (3) and divided by $S(\nu = 1\text{ THz})$ are shown in Figure 2 by symbols corresponding to the ones in Figure 3. The uncertainties are estimated from the asymmetry of THz divergence diagrams, see Figure 3. The dependence $S(\nu)$ decreases monotonically as the frequency ν grows. Therefore, the frequency $\nu_{\max}$ of the maximum in THz spectrum is below 0.5 THz.

We compare the spectral power S estimated from Equation (3) with the spectrum measured by EOS and shown in Figure 2 by the black curve. Both spectra are normalized to the spectral power at $\nu = 1$ THz, at which the spectral maximum in the EOS measurement is achieved. In the range of frequencies $\nu = 1$–2 THz the spectral powers obtained by the two methods coincide within an error. At the highest frequency $\nu = 3$ THz, the spectral power reconstructed from THz angular distribution exceeds the one measured by EOS by approximately two orders of magnitude due to ZnTe phonon band at $\nu \gtrsim 3$ THz [59].

However, the spectral power measured by EOS at $\nu = 0.5$ THz is an order of magnitude lower than the one obtained from integration of the angular distribution (compare the black curve at $\nu = 0.5$ THz with the red square in Figure 2). The overall collection angle of the THz collimatimg lens (Figure 1b) is about $30°$. Therefore, only a little portion of THz emission from the two-color filament escapes the lens and, hence, the ZnTe crystal (Figure 3a). The depletion at $\nu = 0.5$ THz in the THz spectrum measured by EOS can be formed due to geometrical focusing of THz radiation into the spot larger than the probe beam transverse size. We developed a model of EOS detection technique, which includes the effect of the broadband THz geometrical focusing onto the ZnTe crystal, see Appendix A. Figure 5a shows the EOS spectral sensitivity $\varepsilon(\nu)$, calculated according to this model in our experimental conditions, i.e., for the probe beam, which was apertured down to 1 mm and afterwards propagated for about 50 cm towards the ZnTe crystal. The diffraction of the apertured probe beam forms the $\sim$400-μm in diameter quasi-Gaussian beamlet surrounded by divergent rings (Figure 5b,c). We corrected the measured by EOS spectrum taking into account the EOS sensitivity $\varepsilon(\nu)$, see Figure 2, dotted curve. The depletion in the corrected EOS spectrum vanished at $\nu < 1$ THz in agreement with the spectral power S at $\nu = 0.5$ THz (Figure 2, compare black solid and orange dotted curves). This agreement between the corrected EOS spectrum and the spectrum obtained by the integration over the forward hemisphere confirms our result, that the actual spectrum of

THz emission from two-color filament has the maximum at few hundreds of gigahertz or even less.
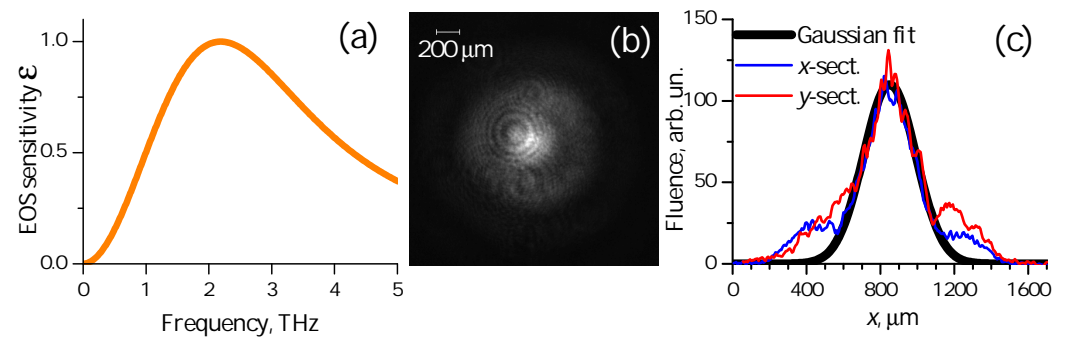

Figure 5. (**a**) Sensitivity of EOS calculated from Equation (A11) assuming Gaussian spatial distribution of the probe beam, $\exp[-r^2/(200\ \mu m)^2]$. (**b**) Spatial fluence distribution of the probe beam on the ZnTe crystal measured by CCD. (**c**) Cross-sections of the probe beam and the Gaussian fit of its most-intense part.

4. Conclusions

In conclusion, the incoherent measurements of the frequency-angular distribution of THz emission from two-color femtosecond filament indicate the monotonic decrease in spectral power from 0.5 to 3 THz and, thus, the absence of spectral maximum in this range. The measured by the rotation of the Golay cell screened by the bandpass filters THz angular distributions were integrated over the forward hemisphere taking into account the filters' transmittance. As a result, we reconstructed the spectral powers at the filters' central frequencies. Our technique of the incoherent measurements of THz spectrum does not use the focusing/collimating THz elements and, therefore, allows us to estimate the actual low-frequency content of THz emission from a two-color filament.

In contrast, the spectrum obtained by electro-optical sampling in the same conditions has a maximum at 1 THz. The depletion of low-frequency components in EOS measurements is due to their geometrical focusing into the spot larger than the probe beam diameter and, therefore, weakening of the THz-induced birefrigence of the probe beam. The model of EOS, which accounts for the nonparaxial diffraction and focusing of THz wave, provides a correction factor to EOS spectrum. The corrected spectrum complies with the incoherent measurements.

Author Contributions: A.A.U., P.A.C., K.A.M. and V.V.B. performed the experiment; D.E.S., N.A.P., I.A.N. and O.G.K. performed the data analysis and developed the model of EOS; V.V.B., S.V.G. and O.G.K. supervized the whole study. All authors have read and agreed to the published version of the manuscript.

Institutional Review Board Statement: Not applicable.

Informed Consent Statement: Not applicable.

Data Availability Statement: Data underlying the results presented in this paper are not publicly available at this time but may be obtained from the authors upon reasonable request.

Conflicts of Interest: The authors declare no conflict of interest.

Appendix A. Derivation of EOS Sensitivity

In this Appendix, we derive the equation for EOS spectral sensitivity following from a finite collection aperture for THz wave and finite transverse and temporal extension of the probe pulse. Here we analyze the THz radiation within the ZnTe transparency window $0.2 \, \text{THz} < \nu < 3 \, \text{THz}$. The iterative method of high-frequency ($\nu > 3 \, \text{THz}$) spectrum reconstruction from EOS measurements was proposed in Ref. [33].

Let t be the time, z the propagation coordinate, x and y the transverse coordinates, $r = \sqrt{x^2 + y^2}$. The electro-optical crystal was $\langle 110 \rangle$ cut, so its main axes are

$$\vec{\xi} = \vec{x}, \quad \vec{\zeta} = \frac{\vec{y} + \vec{z}}{\sqrt{2}}, \quad \vec{\eta} = \frac{\vec{y} - \vec{z}}{\sqrt{2}}. \tag{A1}$$

The cubic crystals like ZnTe, GaP etc. have only six non-zero components of the second-order susceptibility tensor: $\chi^{(2)}_{\xi\zeta\eta} = \chi^{(2)}$ with all possible permutations of indices. Let the incident optical and terahertz fields have only y-components, $L_y(t, r)$ and $T_y(t, r)$, respectively. In this case, the second-order polarization has only x-component, which value at the optical frequency is

$$P_x = 2\chi^{(2)} L_y T_y. \tag{A2}$$

We neglect the linear susceptibility of the crystal and assume it to be thin enough for one-step solution of the propagation equation

$$2ik_L \frac{\partial L_\alpha}{\partial z} = -4\pi k_L^2 P_\alpha, \tag{A3}$$

where α is either x or y, k_L is the wavenumber of optical pulse, so that

$$\begin{pmatrix} L_x \\ L_y \end{pmatrix}^{(out)} = \begin{pmatrix} L_x \\ L_y \end{pmatrix}^{(in)} + 2\pi i k_L \Delta z \begin{pmatrix} P_x \\ P_y \end{pmatrix} = \begin{pmatrix} i\varkappa T_y \\ 1 \end{pmatrix} L_y^{(in)}, \tag{A4}$$

where Δz is the crystal length, $\varkappa = 4\pi k_L \Delta z \chi^{(2)}$.

After the EO crystal, $\lambda/4$ plate is applied:

$$\begin{pmatrix} L_x \\ L_y \end{pmatrix}^{(\lambda/4)} = \frac{1}{2} \begin{pmatrix} 1+i & 1-i \\ 1-i & 1+i \end{pmatrix} \begin{pmatrix} L_x \\ L_y \end{pmatrix}^{(out)}. \tag{A5}$$

Then the Wollaston prism separates the polarizations and direct two beams on the balance detector, which signal is

$$S = \int \left(\left| L_x^{(\lambda/4)} \right|^2 - \left| L_y^{(\lambda/4)} \right|^2 \right) dt\, dx\, dy = -2\varkappa \int T_y \left| L_y^{(in)} \right|^2 dt\, dx\, dy. \tag{A6}$$

Let us now assume that plane THz wave with temporal distribution $T^{(in)}(t)$ [and spectrum $\hat{T}^{(in)}(\omega)$] is focused by an ideal parabolic mirror. The distribution of THz field on the crystal displaced by z from the focus of parabolic mirror can be described by Equation (36) from [60]. We take only scalar axially symmetric part of this non-paraxial solution (the paraxial approach to broadband THz focusing was developed earlier in [61]):

$$\hat{T}_y(\omega, r, z) = -\frac{k}{4} \hat{T}^{(in)}(\omega) \int\limits_0^{\text{asin} \, NA} J_0(kr \sin\theta_s) \exp(-ikz \cos\theta_s) \sin\theta_s d\theta_s, \tag{A7}$$

where $k = \omega/c$, NA is a numerical aperture of the parabola, J_0 is the zeroth order Bessel function, the geometrical focus corresponds to $r = 0$, $z = 0$. This field is now convoluted with the probe beam $\left| L_y^{(in)}(t, r) \right|^2 = L_1(t - t_d) L_2(r)$ where the THz-to-probe delay t_d becomes the only argument of the balance detector signal S.

The Fourier transform of $S(t_d)$ provides the spectrum of THz wave:

$$\hat{S}(\omega_d) \propto \int dt_d \exp(-i\omega_d t_d) \int dt\, r\, dr\, L_1(t - t_d) L_2(r) \int d\omega \exp(i\omega t) \hat{T}_y(\omega, r). \qquad \text{(A8)}$$

The convolutions in time yield a factor $\hat{L}_1(\omega)\delta(\omega - \omega_d)$, so the index in ω_d can be omitted. To eliminate the spatial convolution we introduce Equation (A7) with the substitution $\sigma = \sin\theta_s$:

$$\hat{S}(\omega) \propto k\hat{T}^{(in)}(\omega)\hat{L}_1(\omega) \int r\, dr\, L_2(r) \int\limits_0^{NA} \frac{\sigma d\sigma}{\sqrt{1 - \sigma^2}} J_0(kr\sigma) \exp(-ikz\sqrt{1 - \sigma^2}). \qquad \text{(A9)}$$

The integral over r is the Hankel transform of L_2, so the final equation reads:

$$\hat{S}(\omega) \propto \omega\hat{T}^{(in)}(\omega)\hat{L}_1(\omega) \int\limits_0^{NA} \frac{\sigma d\sigma}{\sqrt{1 - \sigma^2}} \hat{L}_2(\sigma\omega/c) \exp(-iz\sqrt{1 - \sigma^2}\,\omega/c) \qquad \text{(A10)}$$

The spectral sensitivity $\varepsilon(\omega) = \left|\hat{S}(\omega)/\hat{T}^{(in)}(\omega)\right|^2$ can be obtained numerically provided we have the measured spectrum and transverse distribution of the probe.

For the sake of analytical solution, we assume that the crystal is placed exactly in the geometrical focus ($z = 0$), and the probe beam is Gaussian $\left|L_y^{(in)}(t,r)\right|^2 = \exp\left(-(t - t_d)^2/\tau_0^2 - r^2/a_0^2\right)$. Then the Fourier and Hankel transforms as well as the integration are explicit:

$$\frac{\hat{S}(\omega)}{\hat{T}^{(in)}(\omega)} \propto \left[\operatorname{erfi}\varphi - \operatorname{erfi}\left(\varphi\sqrt{1 - NA^2}\right)\right]\exp\left[-\tfrac{1}{4}(\omega\tau_0)^2 - \varphi^2\right] \qquad \text{(A11)}$$

with $\varphi = \omega a_0/(2c)$.

If the crystal cannot be assumed to be thin, the propagation in the medium should be considered carefully [61] and Equation (A6) will be modified to

$$S \propto \int T_y(t,r,z)\left|L_y^{(in)}(t,r,z)\right|^2 dt\, dx\, dy\, dz \qquad \text{(A12)}$$

with additional integration over the crystal length. The solution given by Equation (A12) can be analyzed numerically after substitution of Equation (A7). However, such solution does not have a closed form and depends on too many particular parameters of the experimental setup. This numerical approach makes sense only if one decides to improve the correction for higher THz frequencies, at which the beam distribution varies along the crystal length noticeably.

References

1. Cook, D.; Hochstrasser, R. Intense terahertz pulses by four-wave rectification in air. *Opt. Lett.* **2000**, *25*, 1210–1212. [CrossRef] [PubMed]
2. Kasparian, J.; Sauerbrey, R.; Chin, S.L. The critical laser intensity of self-guided light filaments in air. *Appl. Phys. B* **2000**, *71*, 877. [CrossRef]
3. Kosareva, O.G.; Liu, W.; Panov, N.A.; Bernhardt, J.; Ji, Z.; Sharifi, M.; Li, R.; Xu, Z.; Liu, J.; Wang, Z.; et al. Can we reach very high intensity in air with femtosecond PW laser pulses? *Laser Phys.* **2009**, *19*, 1776–1792. [CrossRef]
4. Mitryukovskiy, S.I.; Liu, Y.; Houard, A.; Mysyrowicz, A. Re-evaluation of the peak intensity inside a femtosecond laser filament in air. *J. Phys. B* **2015**, *48*, 094003. [CrossRef]
5. Braun, A.; Korn, G.; Liu, X.; Du, D.; Squier, J.; Mourou, G. Self-channeling of high-peak-power femtosecond laser-pulses in air. *Opt. Lett.* **1995**, *20*, 73. [CrossRef]
6. Pushkarev, D.; Mitina, E.; Shipilo, D.; Panov, N.; Uryupina, D.; Ushakov, A.; Volkov, R.; Karabutov, A.; Babushkin, I.; Demircan, A.; et al. Transverse structure and energy deposition by a subTW femtosecond laser in air: From single filament to superfilament. *New J. Phys.* **2019**, *21*, 033027. [CrossRef]

7. Apeksimov, D.; Bukin, O.; Bykova, E.; Geints, Y.E.; Golik, S.; Zemlyanov, A.; Il'in, A.; Kabanov, A.; Matvienko, G.; Oshlakov, V.; et al. Filamentation of the focused Ti: Sapphire laser pulse in air at two harmonics. *Plasma Phys. Rep.* **2013**, *39*, 1074–1081. [CrossRef]

8. Théberge, F.; Liu, W.; Simard, P.T.; Becker, A.; Chin, S.L. Plasma density inside a femtosecond laser filament in air: Strong dependence on external focusing. *Phys. Rev. E* **2006**, *74*, 036406. [CrossRef]

9. Ionin, A.A.; Kudryashov, S.I.; Seleznev, L.V.; Sinitsyn, D.V. Tunneling Ionization of Air in the Strong Field of Femtosecond Laser Pulses. *JETP Lett.* **2009**, *90*, 181–185. [CrossRef]

10. Fuji, T.; Suzuki, T. Generation of sub-two-cycle mid-infrared pulses by four-wave mixing through filamentation in air. *Opt. Lett.* **2007**, *32*, 3330–3332. [CrossRef]

11. Thomson, M.D.; Blank, V.; Roskos, H.G. Terahertz white-light pulses from an air plasma photo-induced by incommensurate two-color optical fields. *Opt. Express* **2010**, *18*, 23173–23182. [CrossRef]

12. Matsubara, E.; Nagai, M.; Ashida, M. Coherent infrared spectroscopy system from terahertz to near infrared using air plasma produced by 10-fs pulses. *J. Opt. Soc. Am. B* **2013**, *30*, 1627–1630. [CrossRef]

13. Borodin, A.V.; Panov, N.A.; Kosareva, O.G.; Andreeva, V.A.; Esaulkov, M.N.; Makarov, V.A.; Shkurinov, A.P.; Chin, S.L.; Zhang, X.C. Transformation of terahertz spectra emitted from dual-frequency femtosecond pulse interaction in gases. *Opt. Lett.* **2013**, *38*, 1906. [CrossRef]

14. Oh, T.; You, Y.; Jhajj, N.; Rosenthal, E.; Milchberg, H.; Kim, K.Y. Intense terahertz generation in two-color laser filamentation: Energy scaling with terawatt laser systems. *New J. Phys.* **2013**, *15*, 075002. [CrossRef]

15. Gorodetsky, A.; Koulouklidis, A.D.; Massaouti, M.; Tzortzakis, S. Physics of the conical broadband terahertz emission from two-color laser-induced plasma filaments. *Phys. Rev. A* **2014**, *89*, 033838. [CrossRef]

16. Andreeva, V.; Kosareva, O.; Panov, N.; Shipilo, D.; Solyankin, P.; Esaulkov, M.; de Alaiza Martínez, P.G.; Shkurinov, A.; Makarov, V.; Bergé, L.; et al. Ultrabroad terahertz spectrum generation from an air-based filament plasma. *Phys. Rev. Lett.* **2016**, *116*, 063902. [CrossRef]

17. Fedorov, V.Y.; Tzortzakis, S. Extreme THz fields from two-color filamentation of midinfrared laser pulses. *Phys. Rev. A* **2018**, *97*, 063842. [CrossRef]

18. You, Y.; Oh, T.; Kim, K. Off-axis phase-matched terahertz emission from two-color laser-induced plasma filaments. *Phys. Rev. Lett.* **2012**, *109*, 183902. [CrossRef]

19. Borodin, A.V.; Esaulkov, M.N.; Kuritsyn, I.I.; Kotelnikov, I.A.; Shkurinov, A.P. On the role of photoionization in generation of terahertz radiation in the plasma of optical breakdown. *JOSA B* **2012**, *29*, 1911–1919. [CrossRef]

20. Blank, V.; Thomson, M.; Roskos, H. Spatio-spectral characteristics of ultra-broadband THz emission from two-colour photoexcited gas plasmas and their impact for nonlinear spectroscopy. *New J. Phys.* **2013**, *15*, 075023. [CrossRef]

21. Rasmussen, M.; Jepsen, P.; Zhou, B. Accurately frequency-resolved air-plasma THz beam profile from knifeedge assisted waveform measurements. In Proceedings of the 2021 46th International Conference on Infrared, Millimeter and Terahertz Waves (IRMMW-THz), Chengdu, China, 16–17 August 2021.

22. Sørensen, C.B.; Guiramand, L.; Degert, J.; Tondusson, M.; Skovsen, E.; Freysz, E.; Abraham, E. Conical versus Gaussian terahertz emission from two-color laser-induced air plasma filaments. *Opt. Lett.* **2020**, *45*, 2132–2135. [CrossRef]

23. Ushakov, A.; Chizhov, P.; Andreeva, V.; Panov, N.; Shipilo, D.; Matoba, M.; Nemoto, N.; Kanda, N.; Konishi, K.; Bukin, V.; et al. Ring and unimodal angular-frequency distribution of THz emission from two-color femtosecond plasma spark. *Opt. Express* **2018**, *26*, 18202–18213. [CrossRef]

24. Zhong, H.; Karpowicz, N.; Zhang, X.C. Terahertz emission profile from laser-induced air plasma. *Appl. Phys. Lett.* **2006**, *88*, 261103. [CrossRef]

25. Ushakov, A.; Chizhov, P.; Bukin, V.; Shipilo, D.; Panov, N.; Kosareva, O.; Garnov, S. Multiple Filamentation Effects on THz Radiation Pattern from Laser Plasma in Air. *Photonics* **2021**, *8*, 4. [CrossRef]

26. Li, H.; Zhang, Y.; Sun, W.; Wang, X.; Feng, S.; Ye, J.; Zhang, Y. Contribution of the optical rectification in terahertz radiation driven by two-color laser induced plasma. *Opt. Express* **2020**, *28*, 4810–4816. [CrossRef]

27. Smirnov, S.V.; Kulya, M.S.; Tcypkin, A.N.; Putilin, S.E.; Bespalov, V.G. Detection of the polarization spatial distribution of THz radiation generated by two-color laser filamentation. *Nanosyst.-Phys. Chem. Math.* **2017**, *8*, 613–619. [CrossRef]

28. Hah, J.; Jiang, W.; He, Z.; Nees, J.; Hou, B.; Thomas, A.; Krushelnick, K. Enhancement of THz generation by feedback-optimized wavefront manipulation. *Opt. Express* **2017**, *25*, 17271–17279. [CrossRef]

29. Kolesik, M.; Moloney, J.V. Nonlinear optical pulse propagation simulation: From Maxwell's to unidirectional equations. *Phys. Rev. E* **2004**, *70*, 036604. [CrossRef]

30. Ho, I.C.; Guo, X.; Zhang, X.C. Design and performance of reflective terahertz air-biased-coherent-detection for time-domain spectroscopy. *Opt. Express* **2010**, *18*, 2872–2883. [CrossRef]

31. Dai, J.; Clough, B.; Ho, I.C.; Lu, X.; Liu, J.; Zhang, X.C. Recent progresses in terahertz wave air photonics. *IEEE Trans. Terahertz Sci. Technol.* **2011**, *1*, 274–281. [CrossRef]

32. Xie, J.; Fan, W.H.; Chen, X. Systematic experimental study on a highly efficient terahertz source based on two-color laser-induced air plasma. *Laser Phys.* **2016**, *26*, 055002. [CrossRef]

33. Koulouklidis, A.; Fedorov, V.Y.; Tzortzakis, S. Spectral bandwidth scaling laws and reconstruction of THz wave packets generated from two-color laser plasma filaments. *Phys. Rev. A* **2016**, *93*, 033844. [CrossRef]

34. Rodriguez, G.; Dakovski, G.L. Scaling behavior of ultrafast two-color terahertz generation in plasma gas targets: Energy and pressure dependence. *Opt. Express* **2010**, *18*, 15130–15143. [CrossRef] [PubMed]

35. Zhao, J.; Chu, W.; Wang, Z.; Peng, Y.; Gong, C.; Lin, L.; Zhu, Y.; Liu, W.; Cheng, Y.; Zhuang, S.; et al. Strong spatial confinement of terahertz wave inside femtosecond laser filament. *ACS Photonics* **2016**, *3*, 2338–2343. [CrossRef]

36. Chen, Y.; Marceau, C.; Génier, S.; Théberge, F.; Châteauneuf, M.; Dubois, J.; Chin, S.L. Elliptically polarized Terahertz emission through four-wave mixing in a two-color filament in air. *Opt. Commun.* **2009**, *282*, 4283–4287. [CrossRef]

37. Akhmedzhanov, R.; Ilyakov, I.; Mironov, V.; Suvorov, E.; Fadeev, D.; Shishkin, B. Plasma mechanisms of pulsed terahertz radiation generation. *Radiophys. Quantum Electron.* **2009**, *52*, 482–493. [CrossRef]

38. Wang, T.J.; Marceau, C.; Chen, Y.; Yuan, S.; Théberge, F.; Châteauneuf, M.; Dubois, J.; Chin, S.L. Terahertz emission from a dc-biased two-color femtosecond laser-induced filament in air. *Appl. Phys. Lett.* **2010**, *96*, 211113. [CrossRef]

39. Zhang, X.C.; Xu, J. *Introduction to THz Wave Photonics*; Springer: New York, NY, USA, 2010; Volume 29.

40. Dai, J.; Xie, X.; Zhang, X.C. Detection of broadband terahertz waves with a laser-induced plasma in gases. *Phys. Rev. Lett.* **2006**, *97*, 103903. [CrossRef]

41. Lu, Z.; Campbell, P.; Zhang, X.C. Free-space electro-optic sampling with a high-repetition-rate regenerative amplified laser. *Appl. Phys. Lett.* **1997**, *71*, 593–595. [CrossRef]

42. Ushakov, A.; Panov, N.; Chizhov, P.; Shipilo, D.; Bukin, V.; Savel'ev, A.; Garnov, S.; Kosareva, O. Waveform, spectrum, and energy of backward terahertz emission from two-color femtosecond laser induced microplasma. *Appl. Phys. Lett.* **2019**, *114*, 081102. [CrossRef]

43. Shipilo, D.; Nikolaeva, I.; Pushkarev, D.; Rizaev, G.; Mokrousova, D.; Koribut, A.; Grudtsyn, Y.; Panov, N.A.; Seleznev, L.; Liu, W.; et al. Balance of emission from THz sources in DC-biased and unbiased filaments in air. *Opt. Express* **2021**, *29*, 40687–40698. [CrossRef]

44. Baxter, J.B.; Guglietta, G.W. Terahertz spectroscopy. *Anal. Chem.* **2011**, *83*, 4342–4368. [CrossRef]

45. Wu, Q.; Zhang, X.C. Design and characterization of traveling-wave electrooptic terahertz sensors. *IEEE J. Sel. Top. Quantum Electron.* **1996**, *2*, 693–700.

46. Zhong, H.; Redo, A.; Chen, Y.; Zhang, X.C. THz wave standoff detection of explosive materials. In Proceedings of the Terahertz for Military and Security Applications IV, Orlando, FL, USA, 19 May 2006; SPIE, the International Society for Optics and Photonics: Bellingham, WA, USA, 2006; Volume 6212, p. 62120L.

47. Usami, M.; Yamashita, M.; Fukushima, K.; Otani, C.; Kawase, K. Terahertz wideband spectroscopic imaging based on two-dimensional electro-optic sampling technique. *Appl. Phys. Lett.* **2005**, *86*, 141109. [CrossRef]

48. Mankova, A.; Borodin, A.; Kargovsky, A.; Brandt, N.; Luo, Q.; Sakodynskaya, I.; Wang, K.; Zhao, H.; Chikishev, A.Y.; Shkurinov, A.; et al. Terahertz time-domain and FTIR spectroscopic study of interaction of α-chymotrypsin and protonated tris with 18-crown-6. *Chem. Phys. Lett.* **2013**, *560*, 55–59. [CrossRef]

49. Bergé, L.; Kaltenecker, K.; Engelbrecht, S.; Nguyen, A.; Skupin, S.; Merlat, L.; Fischer, B.; Zhou, B.; Thiele, I.; Jepsen, P.U. Terahertz spectroscopy from air plasmas created by two-color femtosecond laser pulses: The ALTESSE project. *EPL (Europhys. Lett.)* **2019**, *126*, 24001. [CrossRef]

50. THz Band Pass Filters. Available online: www.tydexoptics.com/products/thz_assemblies/thz_band_pass_filter/ (accessed on 22 July 2021).

51. Nikolaeva, I.; Shipilo, D.; Pushkarev, D.; Rizaev, G.; Mokrousova, D.; Koribut, A.; Grudtsyn, Y.; Panov, N.; Seleznev, L.; Liu, W.; et al. Flat-top THz directional diagram of a DC-biased filament. *Opt. Lett.* **2021**, *46*, 5497–5500. [CrossRef]

52. Hansen, R.C. *Phased Array Antennas*; John Wiley & Sons: Hoboken, NJ, USA, 2009; Volume 213.

53. D'Amico, C.; Houard, A.; Franco, M.; Prade, B.; Mysyrowicz, A.; Couairon, A.; Tikhonchuk, V. Conical forward THz emission from femtosecond-laser-beam filamentation in air. *Phys. Rev. Lett.* **2007**, *98*, 235002. [CrossRef]

54. D'Amico, C.; Houard, A.; Akturk, S.; Liu, Y.; Le Bloas, J.; Franco, M.; Prade, B.; Couairon, A.; Tikhonchuk, V.; Mysyrowicz, A. Forward THz radiation emission by femtosecond filamentation in gases: Theory and experiment. *New J. Phys.* **2008**, *10*, 013015.

55. Panov, N.A.; Kosareva, O.G.; Andreeva, V.; Savel'ev, A.; Uryupina, D.S.; Volkov, R.V.; Makarov, V.; Shkurinov, A.P. Angular distribution of the terahertz radiation intensity from the plasma channel of a femtosecond filament. *JETP Lett.* **2011**, *93*, 638. [CrossRef]

56. Orlova, E.; Hovenier, J.; Klaassen, T.; Kašalynas, I.; Adam, A.; Gao, J.; Klapwijk, T.; Williams, B.; Kumar, S.; Hu, Q.; et al. Antenna model for wire lasers. *Phys. Rev. Lett.* **2006**, *96*, 173904. [CrossRef] [PubMed]

57. Klarskov, P.; Strikwerda, A.C.; Iwaszczuk, K.; Jepsen, P.U. Experimental three-dimensional beam profiling and modeling of a terahertz beam generated from a two-color air plasma. *New J. Phys.* **2013**, *15*, 075012. [CrossRef]

58. Panov, N.; Andreeva, V.; Kosareva, O.; Shkurinov, A.; Makarov, V.; Bergé, L.; Chin, S. Directionality of terahertz radiation emitted from an array of femtosecond filaments in gases. *Laser Phys. Lett.* **2014**, *11*, 125401. [CrossRef]

59. Gallot, G.; Zhang, J.; McGowan, R.; Jeon, T.I.; Grischkowsky, D. Measurements of the THz absorption and dispersion of ZnTe and their relevance to the electro-optic detection of THz radiation. *Appl. Phys. Lett.* **1999**, *74*, 3450–3452. [CrossRef]

60. Varga, P.; Török, P. Focusing of electromagnetic waves by paraboloid mirrors. I. Theory. *J. Opt. Soc. Am. A* **2000**, *17*, 2081–2089. [CrossRef]

61. Ahi, K. Mathematical modeling of THz point spread function and simulation of THz imaging systems. *IEEE Trans. Terahertz Sci. Technol.* **2017**, *7*, 747–754. [CrossRef]